A GSVD-Based Precoding Scheme for MIMO-NOMA Relay Transmission

Chenguang Rao, Zhiguo Ding, *Fellow, IEEE*, Kanapathippillai Cumanan, *Senior Member, IEEE* and Xuchu Dai

Abstract—Recently, the multiple-input multiple-output (MIMO) non-orthogonal multiple-access (NOMA) transmission, denoted as MIMO-NOMA, has been widely applied for Internet-of-Things (IoT) systems due to its spectral efficiency. As a promising precoding method, the generalized singular value decomposition (GSVD) based precoding scheme has been studied in MIMO-NOMA. In this study, we apply the GSVD-based precoding scheme to a downlink MIMO-NOMA communication system with an amplify-and-forward (AF) relay and two IoT users. A closed-form expression of the probability density function (PDF) of two channel matrices' generalized singular values (GSVs) is obtained in order to facilitate the performance analysis for cooperative MIMO-NOMA transmission. In particular, by this distribution characteristic result, the users' rates and outage probabilities achieved by MIMO-NOMA are studied for the insightful performance evaluation. In addition, the asymptotic approximations for outage probabilities at the high signal-to-noise-ratio (SNR) condition are presented. In addition to characterize the performance achieved by cooperative MIMO-NOMA, resource allocation for the addressed NOMA system is also investigated in this paper, where a suboptimal power allocation algorithm to maximize the sum rate is given. The solution obtained by the proposed algorithm is studied, where the optimality condition of the solution is obtained. Finally, simulation results are presented to show the superiority of the scheme and verify these analytical results.

Index Terms—Amplify-and-forward (AF) relay, generalized singular value decomposition(GSVD), internet of things (IoT), multiple-input multiple-output (MIMO), non-orthogonal multiple access (NOMA).

I. INTRODUCTION

A. Related works and the Motivation.

With the rapidly development of internet of things (IoT), there is an urgent need for high-quality wireless communication systems. Among the potential enabling technologies for future IoT networks, multiple-input multiple-output (MIMO), a technology with high spectral efficiency, has been regarded as a crucial technology and has got broad application [1]–[4]. In addition, MIMO systems usually combine with non-orthogonal multiple access (NOMA) for rational use of the spectrum, which is termed the MIMO-NOMA technology and has been widely studied and applied [5]–[8]. However, in

C. Rao and X. Dai are with the CAS Key Laboratory of Wireless-Optical Communications, University of Science and Technology of China, No.96 Jinzhai Road, Hefei, Anhui Province, 230026, P. R. China. (e-mail: rcg1839@mail.ustc.edu.cn; daixc@ustc.edu.cn).

Z. Ding is with Department of Electrical Engineering and Computer Science, Khalifa University, Abu Dhabi, UAE. (e-mail:, zhiguo.ding@ieee.org).

Kanapathippillai Cumanan is with the School of Physics, Engineering and Technology, University of York, York YO10 5DD, U.K. (e-mail: kanapathippillai.cumanan@york.ac.uk).

the long distance communication, the feasible transmission distance between the base station and the IoT devices or users may not support a stable and efficient communication condition, in which case a relay station is required to improve link quality [9]. This promotes the development of cooperative MIMO-NOMA transmission research [10]–[12]. The relaying techniques can be classified into two types: amplify-and-forward (AF) relaying and decode-and-forward (DF) relaying. Compared with DF, AF has a simpler implementation and a lower dissipation [13], which make it more attractive in practice. The precoding schemes of MIMO with an AF relay can be developed from conventional MIMO transmissions, which have been studied in [14]–[16]. There are mainly two types for MIMO precoding schemes: non-linear precoding [17]–[19] and linear precoding [20], [21]. The non-linear precoding is too complex to be often employed in practice, while linear precoding schemes can better balance efficiency and complexity and thus have been extensive used. The generalized singular value decomposition (GSVD) has stood out among the linear precoding schemes because of its implementation simplicity and advantageous performance, especially when the signal-to-noise-ratio (SNR) is high [22]–[24]. In the MIMO-NOMA-GSVD-based scheme, the channel matrices of two users are diagonalized simultaneously to achieve the purpose of transforming an MIMO channel into several parallel single-input single-output (SISO) channels. Then the NOMA principle can be applied to each SISO channel individually. In [23], the authors have studied a GSVD-based two-user MIMO-NOMA download communication system. In [25], the authors have analyzed the perturbation of GSVD-NOMA scheme with imperfect channel state information. In [24], the authors have considered the performance of GSVD-NOMA from the single channel perspective, where the distribution characteristic of the ordered GSVD has been analyzed. In [26], the GSVD-NOMA scheme with the security constraint has been studied. In [22] and [27], the authors have studied the GSVD-based MIMO-NOMA system with a DF relay.

All works above have contributed to the GSVD-based MIMO-NOMA schemes. However, to the best knowledge of the authors, the design of GSVD-based MIMO-NOMA with an AF relay is still unknown, which motivates our work in this paper. The key contribution of this work is how to characterize the distribution characteristic of the generalized singular values (GSVs) of two channel matrices, which is needed for the performance analysis of the scheme. In [23], the probability density functions (PDFs) of two Gaussian random matrices are calculated for both the two-user downlink MIMO-NOMA scenario and MIMO-NOMA scenario with a DF relay. In the DF relay scenario, the relay station can decode the received messages and then encode the message before

relaying. Thus, its end-to-end matrices can be decomposed into several Gaussian matrices, and the distribution characteristics of GSVs of these Gaussian channel matrices can be directly obtained from existing works for the performance analysis. However, in the AF relay scenario, the channel matrices are the products of Gaussian matrices and no longer satisfy the Gaussian distribution. As a result, those existing results about GSVD-NOMA in [23] cannot be applied. Thus, we are devoted to finding a new approach to solve this problem in this paper.

B. Contributions

In this paper, we consider a two-user downlink MIMO-NOMA scenario with a single AF relay station and two IoT users. The far user, i.e., the user which is farther from the base station, receives messages via the AF relay station, while the near user, i.e., the user which is close to the base station, receives messages directly from the base station. Then the end-to-end channel matrix pair consists of a Gaussian random matrix and a new matrix which is a product between two Gaussian random matrices. We calculate the distribution characteristics of the corresponding GSVs for the channel matrix pair and then analyze the performance of the communication system by using these results.

The main contributions of this paper are shown as follows:

- A GSVD-based MIMO-NOMA IoT transmission system with an AF relay precoding scheme is presented. Specifically, the GSVD-based precoding scheme is applied to this system. The distribution characteristic of the GSVs of two channel matrices of the considered scenario is analyzed. Closed-form expressions of both the PDF and marginal PDF of GSVs are obtained.

- Based on the PDF of GSVs, the performance analysis for the considered cooperative MIMO-NOMA scheme is carried out. In particular, the expressions of average rates and outage probabilities are obtained. Besides, the asymptotic results at high SNR are also estimated.

- To maximize the sum rate of two users and meet those communication quality requirements, a problem where the objective function is the sum rate of the two users is generated. As the solution of this problem, a suboptimal algorithm is proposed. Furthermore, this solution is proved to be optimal in most cases in practice.

The rest of this paper is organized as follows. In Section II, we briefly describe the system model and the GSVD-based precoding scheme. In Section III, we present the performance analysis of the system. In Section IV, we study the power allocation strategy to get the maximum sum rate and give a suboptimal power allocation algorithm. Simulation results are provided in Section V, and conclusions are presented in Section VI.

II. SYSTEM MODEL

A. System Setup and Parameters

Consider an AF-relay assisted downlink MIMO-NOMA transmission system as Fig. 1. We denote the base station, the relay station and the two IoT users by BS, R and U_i, $i = 1, 2$,

TABLE I
NOTATIONS AND PARAMETER DEFINITIONS OF THE SYSTEM MODEL.

| Notations	Definitions
$\mathbf{X}$	Matrix
$\mathbf{x}$	Column vector
$\{X_{m,n}\}$	The m-th, n-th element of $\mathbf{X}$
$\mathbb{C}, \mathbb{R}$	Complex number field, real number field
$E(.)$	Expectation
trace$(.)$	Trace
det$(.)$	Determinant
Pr$()$	Probability calculation
$\mathbf{I}$	Identity matrix
$G(.)$	Meijer G-function
ξ_i	Permutations
$sign(\xi_i)$	Sign function of permutations
$U(.)$	Tricomi confluent hypergeometric function
$\mathbf{H}_i$	Channel matrices
U_i, BS	Communication nodes
d_i	Distances between nodes
M, N_i	Numbers of antennas
$\mathbf{s}, \mathbf{s}_i$	Message vectors
$\mathbf{P}_s, \mathbf{D}_i$	Precoding and decoding matrices
P_0, P_R	Transmission powers
t_0, t_R	Power normalization coefficients
l_i	Power allocation coefficients
$\mathbf{n}, \mathbf{n}_i$	White noises
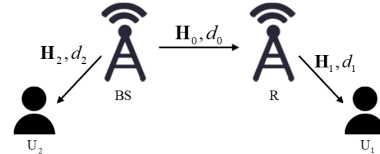
Fig. 1. System model.

respectively. [1] In this system model, U_1 represents a 'poor channel' user that is far from BS. The poor communication condition of U_1 blue to the requirement of relay station R. [2] Recall that NOMA performs better when the difference between the users' conditions is larger. Therefore, U_1 is paired with a 'good channel' user, U_2, whose communication condition is good enough to support direct communication to BS. The distances between BS and R, R and U_1, BS and U_2 are denoted by d_0, d_1, d_2, respectively. The distances are assumed to satisfy d_0, d_1, $d_2 > 1$, d_0, $d_1 > d_2$. The distance between R and U_2 is assumed to be large enough to ignore the interference each other. BS and U_i are equipped with N_B and N_i antennas, respectively. R is equipped with M antennas. Denote $N = \min\{N_B, N_1, N_2\}$. The numbers of antennas satisfy that $M \geq N$ [3]. $\mathbf{H}_0 \in \mathbb{C}^{M \times N}$ is the downlink channel matrix between BS and R, $\mathbf{H}_1 \in \mathbb{C}^{N \times M}$ is the downlink channel matrix between R and U_1, and $\mathbf{H}_2 \in \mathbb{C}^{N \times N}$ is the downlink channel matrix between BS and U_2. In this

---

[1] For the case with more than two users, a hybrid approach can be employed in which users are divided into groups of two users, each group is allocated orthogonal resources, and within each two-user group, the proposed GSVD-based MIMO-NOMA scheme can be utilized.

[2] When there is a direct link between U_1 and BS, the system can be simplified to a GSVD-MIMO scenario. The detailed analysis can be found in [23].

[3] This condition is to ensure the full rank of the channel matrix for subsequent analyses.

paper, the number of the multipath propagation is assumed to be very large, and the channel matrices can be modeled as independent and identically complex Gaussian random matrices [28], whose all elements have zero means and one variances. The large scale fading coefficient corresponding to channel matrix $\mathbf{H}_i$ is modeled as $1/\sqrt{d_i^\tau}$, $i = 0, 1, 2$, where τ represents the path loss exponent. The message broadcasted by BS is expressed as $\mathbf{x} = \sqrt{P_0}\mathbf{P}_s\mathbf{s}$. $\mathbf{P}_s$ represents the precoding matrix. $\mathbf{s} = l_1\mathbf{s}_1 + l_2\mathbf{s}_2$, where $\mathbf{s}_i$ is the signal vector for U_i, $E(\mathbf{s}_i\mathbf{s}_i^H) = \mathbf{I}$. P_0 is the transmission power. l_i denotes the power allocation coefficient and satisfies $l_1^2 + l_2^2 = 1$. Then the received message at R and U_2 can be expressed as follows:

$$
\begin{cases}
\mathbf{y}_R = \dfrac{\sqrt{P_0}}{t_0\sqrt{d_0^\tau}}\mathbf{H}_0\mathbf{P}_s\mathbf{s} + \mathbf{n}_0, \\
\mathbf{y}_2 = \dfrac{\sqrt{P_0}}{t_0\sqrt{d_2^\tau}}\mathbf{D}_2\mathbf{H}_2\mathbf{P}_s\mathbf{s} + \mathbf{D}_2\mathbf{n}_2
\end{cases}, \quad (1)
$$

respectively. t_0 denotes the long-term power normalization coefficient (see (9)) to reduce the power gap between the various channels, and $\mathbf{D}_2$ denotes the decoding matrix at U_2. Each element of $\mathbf{n}_i$, $i = 0, 1, 2$ is independent white noise with unit variance. In this paper, it is assumed that all of the white noises have the same variances N_0. Then R sends $\frac{\sqrt{P_R}}{t_R}\mathbf{y}_R$ to U_1. P_R is the transmission power at R. To keep the average power on each antenna within the power limit, the average normalization coefficient t_R is set as the average power of $\mathbf{y}_R$, which can be expressed as follows:

$$
t_R = \sqrt{E\{\text{trace}(\mathbf{H}_0\mathbf{H}_0^H)\}\frac{P_0}{t_0^2 d_0^\tau} + N_0}. \quad (2)
$$

From [29], it can be shown that

$$
E\{\text{trace}(\mathbf{H}_0\mathbf{H}_0^H)\} = MN. \quad (3)
$$

Therefore, t_R can be simplified as follows:

$$
t_R = \sqrt{MN\frac{P_0}{t_0^2 d_0^\tau} + N_0}. \quad (4)
$$

From (1), the received message at U_i can be expressed as follows:

$$
\begin{cases}
\mathbf{y}_1 = \dfrac{\sqrt{P_0 P_R}}{t_0 t_R\sqrt{d_0^\tau d_1^\tau}}\mathbf{D}_1\mathbf{H}_1\mathbf{H}_0\mathbf{P}_s\mathbf{s} + \dfrac{\sqrt{P_R}}{t_R\sqrt{d_1^\tau}}\mathbf{D}_1\mathbf{H}_1\mathbf{n}_0 + \mathbf{D}_1\mathbf{n}_1 \\
\mathbf{y}_2 = \dfrac{\sqrt{P_0}}{t_0\sqrt{d_2^\tau}}\mathbf{D}_2\mathbf{H}_2\mathbf{P}_s\mathbf{s} + \mathbf{D}_2\mathbf{n}_2
\end{cases}, \quad (5)
$$

where $\mathbf{D}_1$ denotes the decoding matrix at U_1.

B. Application of GSVD

The design for $\mathbf{P}_s$ and $\mathbf{D}_i$ is considered in this subsection. To diagonalize the channel matrices simultaneously for eliminating the interference between subchannels, the GSVD-based precoding scheme is applied [23]. From [30], the GSVD is adopted to the matrix pair $\{\mathbf{H}_1\mathbf{H}_0, \mathbf{H}_2\}$ as follows [30]:

$$
\mathbf{H}_1\mathbf{H}_0 = \mathbf{U}_1\mathbf{\Sigma}_1\mathbf{V}, \ \mathbf{H}_2 = \mathbf{U}_2\mathbf{\Sigma}_2\mathbf{V}, \quad (6)
$$

where $\mathbf{U}_i \in \mathbb{C}^{N\times N}$ is a unitary matrix, and $\mathbf{V} \in \mathbb{C}^{N\times N}$ is an invertible matrix. $\mathbf{\Sigma}_i = diag(\mu_{i,1}, ..., \mu_{i,N})$ that satisfying

$\mu_{1,q}^2 + \mu_{2,q}^2 = 1$, $\forall 1 \leq q \leq N$. The generalized singular values (GSV) are defined as $\omega_q = \mu_{1,q}^2/\mu_{2,q}^2$, $q = 1, 2, ..., N$. On the other hand, it can be shown that $\mu_{1,q}^2 = \omega_q/(1 + \omega_q)$, $\mu_{2,q}^2 = 1/(1 + \omega_q)$.

By applying GSVD, the precoding and decoding matrices can be designed as $\mathbf{P}_s = \mathbf{V}^{-1}$ and $\mathbf{D}_i = \mathbf{U}_i^H$. The expressions of (5) can be rewritten as follows:

$$
\begin{cases}
\mathbf{y}_1 = \dfrac{\sqrt{P_0 P_R}}{t_0 t_R\sqrt{d_0^\tau d_1^\tau}}\mathbf{\Sigma}_1\mathbf{s} + \dfrac{\sqrt{P_R}}{t_R\sqrt{d_1^\tau}}\mathbf{n}_0' + \mathbf{n}_1' \\
\mathbf{y}_2 = \dfrac{\sqrt{P_0}}{t_0\sqrt{d_2^\tau}}\mathbf{\Sigma}_2\mathbf{s} + \mathbf{n}_2'
\end{cases}. \quad (7)
$$

Since the unitary matrices do not change the distribution of Gaussian matrices, it can be shown that $\mathbf{n}_i' = \mathbf{U}_i^H\mathbf{n}_i$, $i = 1, 2$, is also a white Gaussian distributed vector. In addition, each element of $\mathbf{n}_0' = \mathbf{U}_1^H\mathbf{H}_1\mathbf{n}_0$ is the inner product of two independent Gaussian random vectors with zero means and diagonal covariance matrices. We denote $n_{i,q}'$ by the q-th element of $\mathbf{n}_i'$. Then it is obvious that $E\{n_{1,q}'^2\} = E\{n_{2,q}'^2\} = N_0$. As for $n_{0,q}'$, we rewrite it as $n_{0,q}' = \sum_{j=1}^N a_j b_j$, where a_j, b_j are independent Gaussian random variables with zero means and unit variances. Then, its power can be obtained as follows:

$$
E\{n_{0,q}'^2\} = E\{(\sum_{j=1}^N a_j b_j)^2\} = E\{\sum_{j=1}^N a_j^2 b_j^2\} = NN_0. \quad (8)
$$

Similar to t_R, the normalization coefficient t_0 is set as the average power of $\mathbf{P}_s\mathbf{s}$, which can be designed as $t_0^2 = E\{\text{trace}(\mathbf{V}\mathbf{s}\mathbf{s}^H\mathbf{V}^H)\} = E\{\text{trace}(\mathbf{V}\mathbf{V}^H)\}$. From [23], it can be shown that

$$
t_0^2 = E\{\text{trace}(\mathbf{V}\mathbf{V}^H)\} = \frac{N}{2N - N} = 1. \quad (9)
$$

This result shows that when the antennas at both ends are equal, the long-term average power of each channel is approximately equal, so normalization coefficient is not needed.

The q-th element of $\mathbf{y}_i$ can be expressed as follows:

$$
\begin{cases}
y_{1,q} = \dfrac{\sqrt{P_0 P_R}}{t_R\sqrt{d_0^\tau d_1^\tau}}\mu_{1,q}(l_1 s_{1,q} + l_2 s_{2,q}) + \dfrac{\sqrt{P_R}}{t_R\sqrt{d_1^\tau}}n_{0,q}' + n_{1,q}' \\
y_{2,q} = \dfrac{\sqrt{P_0}}{\sqrt{d_2^\tau}}\mu_{2,q}(l_1 s_{1,q} + l_2 s_{2,q}) + n_{2,q}
\end{cases}, \quad (10)
$$

where $s_{i,q}$ is the q-th element of $\mathbf{s}_i$. (10) also represents the q-th SISO channel between BS and U_i. We denote signal-to-interference-plus-noise-ratio (SINR) of $s_{p,q}$ at U_i as $\gamma_{p\to i,q}$. The SINR is defined as the ratio of the power of the required message to the sum of the power of interference and noise. As the Shannon–Hartley theorem, its relation to the rate $r_{i,q}$ is expressed as follows:

$$
r_{i,q} = \log(1 + \gamma_{i\to i,q}). \quad (11)
$$

Since U_2 has a better channel condition (If otherwise, U_1 tends to be chosen as the relay-assisted users.), we apply the successive interference cancellation (SIC) to U_2. In particular, U_2 firstly decodes $\mathbf{s}_1$ by regarding $\mathbf{s}_2$ as noise. Then if $\mathbf{s}_1$ can be decoded correctly, it can be eliminated from the message

and $\mathbf{s}_2$ is decoded without interference. U_1 decodes $\mathbf{s}_1$ by regarding $\mathbf{s}_2$ as noise directly. From (10), $\gamma_{p \to i,q}$ are given by

$$\gamma_{1\to1,q} = \frac{(\frac{\sqrt{P_0 P_R}}{t_R\sqrt{d_0^\tau d_1^\tau}}\mu_{1,q}l_1)^2}{(\frac{\sqrt{P_0 P_R}}{t_R\sqrt{d_0^\tau d_1^\tau}}\mu_{1,q}l_2)^2 + (\frac{\sqrt{P_R}}{t_R\sqrt{d_1^\tau}})^2 N_0 + N_0}, \quad (12)$$

$$\gamma_{1\to2,q} = \frac{(\frac{\sqrt{P_0}}{\sqrt{d_2^\tau}}\mu_{2,q}l_1)^2}{(\frac{\sqrt{P_0}}{\sqrt{d_2^\tau}}\mu_{2,q}l_2)^2 + N_0}, \gamma_{2\to2,q} = \frac{(\frac{\sqrt{P_0}}{\sqrt{d_2^\tau}}\mu_{2,q}l_2)^2}{N_0}. \quad (13)$$

After simplification, the following equations can be derived:

$$\gamma_{1\to1,q} = \frac{l_1^2\omega_q}{(l_2^2 + C_1)\omega_q + C_1}. \quad (14)$$

$$\gamma_{1\to2,q} = \frac{l_1^2}{C_2\omega_q + C_2 + l_2^2}, \gamma_{2\to2,q} = \frac{l_2^2}{C_2\omega_q + C_2}, \quad (15)$$

where

$$C_1 = \frac{d_0^\tau N_0}{P_0} + \frac{t_R^2 d_0^\tau d_1^\tau N_0}{P_0 P_R}, C_2 = \frac{d_2^\tau N_0}{P_0}. \quad (16)$$

III. PERFORMANCE ANALYSIS

In this section, we first consider the distribution characteristics of $\omega = \frac{1}{N}\sum_{q=1}^{N}\omega_q$, including its joint and marginal PDF. Then we use the results to analyze the average achievable rates and outage probabilities of two users.

A. The Distribution Characteristic of ω

Since all metrics for performance analysis are functions of ω, it is necessary to find the PDF of ω first. In this subsection, firstly, we construct a matrix with eigenvalues equal to GSVs and then obtain the joint PDF of its eigenvalues from the existing conclusion. Naturally, we can obtain the joint PDF of $\omega_1, \omega_2, ..., \omega_N$ right away. Then we can obtain the marginal PDF via integral operations.

Theorem 1. *The unordered joint PDF of $\omega_1, \omega_2, ..., \omega_N$ can be expressed as follows:*

$$f(\omega_1, \omega_2, ..., \omega_N) = \frac{1}{V}\prod_{1\le m<n\le N}(\omega_n - \omega_m)\det(\{G_{m,n}\}), \quad (17)$$

where

$$G_{m,n} = G_{1,2}^{2,1}\left(\begin{matrix}-N\\M+m-N-1, 0\end{matrix}\Big|\omega_n\right). \quad (18)$$

G is the Meijer G-function [31]. The normalization factor V can be expressed as follows:

$$V = N\Gamma(M)\prod_{i=1}^{N}i^{4(N-i)}. \quad (19)$$

Proof. See Appendix A. □

Then we need to obtain the marginal PDF for further analysis. We can directly obtain marginal PDF based on joint PDF via integral operations, as shown in the following theorem:

Theorem 2. *The marginal PDF of ω can be expressed as follows:*

$$g(\omega) = \frac{1}{V}\sum_{\xi_1,\xi_2\in S_N} sign(\xi_1)sign(\xi_2)\prod_{o=1}^{N-1}W_o\omega^{\xi_1(N)-1}$$
$$\times G_{1,2}^{2,1}\left(\begin{matrix}-N\\M+\xi_2(N)-N-1, 0\end{matrix}\Big|\omega\right), \quad (20)$$

where

$$W_o = \Gamma(\xi_1(o))\Gamma(M-N+\xi_1(o)+\xi_2(o)-1)$$
$$\times \Gamma(N-\xi_1(o)+1). \quad (21)$$

ξ_1 and ξ_2 are permutations of length N. On the other word, $\xi = (\xi(1), \xi(2), ..., \xi(N))$, $\forall 1 \le a, b \le N$, $a \ne b$, $\xi(a) \in \{1, 2, ..., N\}$, $\xi(a) \ne \xi(b)$. $sign(\xi)$ is equal to -1 if ξ is an odd permutation, otherwise $sign(\xi) = 1$ [24].

Proof. See Appendix B. □

For the special case where each node is equipped with a single antenna, the use of Theorem 1 immediately leads to the following corollary.

Corollary 1. *When $M = N = 1$, the marginal PDF of ω can be expressed as follows:*

$$g(\omega) = U(2, 1, \omega_n), \quad (22)$$

where $U(a, b, x)$ is the Tricomi confluent hypergeometric function [32].

Proof. See Appendix C. □

To illustrate the result of (22) visually, it will be pointed out the relationship between this result and classical single-antenna Rayleigh fading channel model. At the single-antenna condition, the GSV degrades into

$$\omega_0 = \frac{|h_0|^2|h_1|^2}{|h_2|^2}. \quad (23)$$

h_i, $i = 0, 1, 2$ is the independent Rayleigh fading coefficient, which is subject to Gaussian distribution with the zero mean and the unit variance. Then the following remark can be given.

Remark 1. *At the single-antenna condition, the PDF of ω_0 from (23) is equal to the result of (72), i.e.,*

$$g(\omega_0) = U(2, 1, \omega_0). \quad (24)$$

Proof. See Appendix D. □

Remark 1 shows that in the especial case where each node is equipped with a single antenna, $g(\omega)$ will degenerate into the PDF of the random variable $\omega_0 = \frac{|h_0|^2|h_1|^2}{|h_2|^2}$, i.e., the SISO model, which confirms the results in this subsection.

Next, the average rates can be calculated by using the expressions of marginal PDF.

B. Average Achievable Rate

In this subsection, we will obtain the expressions of the average rates of the users by using the marginal PDF of ω.

To evaluate the effectiveness of the system, we need to get the expressions of average achievable rates. According to (11), (14), (15) and (20), the average achievable rates can be written as follows:

$$R_1 = \frac{N}{2} \int_0^{+\infty} \log(\frac{(1+C_1)\omega_q + C_1}{(l_2^2 + C_1)\omega_q + C_1}) g(\omega) d\omega, \qquad (25)$$

$$R_2 = \frac{N}{2} \int_0^{+\infty} \log(\frac{C_2\omega_q + C_2 + l_2^2}{C_2\omega_q + C_2}) g(\omega) d\omega. \qquad (26)$$

According to the definitions, we can get the expressions of average achievable rates as follows:

Theorem 3. *The average achievable rates of two users can be expressed as follows:*

$$R_1 = \frac{N}{2} \log(\frac{C_1+1}{C_1+l_2^2}) + \frac{N}{2} J(\frac{C_1}{C_1+1}) - \frac{N}{2} J(\frac{C_1}{C_1+l_2^2}), \quad (27)$$

$$R_2 = \frac{N}{2} J(1 + \frac{l_2^2}{C_2}) - J(1), \qquad (28)$$

where

$$J(x) = \log x + \sum_{\xi_1, \xi_2 \in S_N} sign(\xi_1)sign(\xi_2) \prod_{o=1}^{N-1} W_o G_{3,4}^{4,2} \\ \left(\begin{matrix} 0, \xi_1(N) - N, 1 \\ 0, 0, M - N + \xi_1(N) + \xi_2(N) - 1, \xi_1(N) \end{matrix} \middle| x \right). \qquad (29)$$

Proof. See Appendix E. □

To maximum the sum rate, a resource allocation optimization scheme can be considered. The explicit expressions obtained in Theorem 3 can be used as the objective function of the optimization problem, as shown in Section IV.

C. Outage Probability

In this subsection, we will obtain the expressions of the outage probabilities of the users by using the marginal PDF of ω.

To evaluate the reliability of the system, it is necessary to calculate the outage probabilities. It is assumed that the target SINR of $\mathbf{s}_i$ is set as T_i. In this paper, the outage probability of U_i is defined as the probability of the event that SIC can not be carried out successfully (only for U_2) or SINR falls short of the target, i.e.

$$P_{out,1} = 1 - \Pr\{\gamma_{1\to1} > T_1\}, \\ P_{out,2} = 1 - \Pr\{\gamma_{1\to2} > T_1, \gamma_{2\to2} > T_2\}. \qquad (30)$$

According to the definition, the following theorem about the outage probabilities achieved by cooperative MIMO-NOMA can be obtained.

Theorem 4. *The outage probability of U_1 can be expressed as follows:*

$$P_{out,1} = \begin{cases} G(D_1), l_2^2 < C_{H,1} \\ 1, l_2^2 \geq C_{H,1} \end{cases}. \qquad (31)$$

The expression of outage probability of U_2 is depended with the parameters, which can be expressed as follows:

- When $C_2 \geq \frac{1}{T_1 + T_2 + T_1 T_2}$,

$$P_{out,2} = 1. \qquad (32)$$

- When $C_2 < \frac{1}{T_1 + T_2 + T_1 T_2}$

$$P_{out,2} = \begin{cases} 1, l_2^2 \leq C_2 T_2 \text{ or } l_2^2 \geq C_{H,2} \\ 1 - G(E), C_2 T_2 \leq l_2^2 \leq C_T \\ 1 - G(D_2^{-1}), C_T \leq l_2^2 \leq C_{H,2} \end{cases}. \qquad (33)$$

The constants are defined as follows:

$$C_{H,i} = \frac{1 - C_i T_1}{T_1 + 1}, C_T = \frac{T_2}{T_1 + T_2 + T_1 T_2}, \\ D_i = \frac{C_i T_1}{-(T_1 + 1)l_2^2 + 1 - C_i T_1}, E = \frac{l_2^2 - C_2 T_2}{C_2 T_2}, \qquad (34)$$

$G(\omega)$ is the indefinite integral of $g(\omega)$. From [33], we can get $G(\omega)$ as follows:

$$G(\omega) = \int_0^\omega g(t)dt \\ = \sum_{\xi_1, \xi_2 \in S_N} sign(\xi_1)sign(\xi_2) \prod_{o=1}^{N-1} W_o \qquad (35) \\ \times G_{2,3}^{2,2} \left(\begin{matrix} 1, \xi_1(N) - N \\ M - N + \xi_1(N) + \xi_2(N) - 1, \xi_1(N), 0 \end{matrix} \middle| \omega \right).$$

Proof. See Appendix F. □

It can be seen from the theorem that sometimes the outage probabilities will be 1, depending on the channel conditions, the power transmission, the number of the antennas, the system requirements, and the power allocation coefficients we choose. The results facilitate how to choose parameters and power allocation coefficients to avoid undesirable situation.

When $P_{out,1}$, $P_{out,2} \not\equiv 1$ and $P_0 \to +\infty$, $P_{out,1}$, $P_{out,2} \to 0$. We are interested in the decay rate when $P_0 \to +\infty$. We analyze them in the next subsection.

D. Asymptotic Analysis

Since the NOMA performs well at high SNR [6], [7], it is meaningful to analyze the asymptotic outage probabilities when $P_0 \to +\infty$. In this subsection, we will obtain the results by studying the asymptotic characteristic of $G(\omega)$. Specifically, we have the following theorem:

Theorem 5. *When $P_0 \to +\infty$, the asymptotic results of P_0 can be expressed as follows:*

$$P_{out,1} \to \frac{1}{P_0}, P_{out,2} \to \frac{1}{P_0}. \qquad (36)$$

Proof. See Appendix G. □

As shown in the theorem, the two users' asymptotic results are equal and independent of other parameters, such as the antenna numbers, the power allocation coefficients or the transmission distances. This result also demonstrates that the proposed scheme is fair to two users.

IV. POWER ALLOCATION FOR SUM RATE MAXIMATION

In this section, we formulate a power allocation problem. To balance the performance of both users, we use the sum rate, i.e., $R_1 + R_2$, as the objective function. In addition, since the minimum rates are often required in communication, the constraints of R_1 and R_2 are need to be considered. Denote the minimum transmission rate required by the system of U_i as $r_i > 0$. Then R_1 and R_2 need to satisfy

$$R_1 \geq r_1,\ R_2 \geq r_2. \tag{37}$$

Besides, to meet reliability requirements, we set the maximum outage probabilities $0 < p_1,\ p_2 \leq 1$. Then $P_{out,1}$ and $P_{out,2}$ need to satisfy

$$P_{out,1} \leq p_1,\ P_{out,2} \leq p_2. \tag{38}$$

Therefore, the addressed resource allocation problem can be formulated as follows:

$$\begin{aligned} P_1:\ &\max_{l_2^2} R_1 + R_2 \\ &\text{s.t. } 0 \leq l_2^2 \leq 1,\ R_1 \geq r_1,\ R_2 \geq r_2, \\ &\quad P_{out,1} \leq p_1,\ P_{out,2} \leq p_2. \end{aligned} \tag{39}$$

In the remainder of the paper, the data rates are defined as $R_1(l_2^2)$ and $R_2(l_2^2)$, in order to highlight the fact that l_2^2 is the optimization variable. For simplicity, we represent l_2^2 as x in the following analysis, i.e., we will use $R_1(x)$ and $R_2(x)$ to denote $R_1(l_2^2)$ and $R_2(l_2^2)$.

Since $R_1(x) + R_2(x)$ is a non-convex function, it is hard to solve. On the other hand, the convexity of $R_1 + R_2$ depends on parameters C_1 and C_2. Therefore, we are going to solve this problem by analyzing the properties of the function $R_1 + R_2$. Specifically, our approach to solve this problem is as follows: First, we focus on the constraints and transform them into one inequality like $x_L \leq x \leq x_H$. Next, we simplify the original objective function to a simpler function of $f(x)$ by removing the terms independent of l_2^2. Then by analyzing the monotonicity of the objective function, we prove that $f(x)$ is a monotonically increasing function under a certain condition, that is to say, $x^* = x_H$ when a condition holds. Otherwise, when the condition does not hold, we offer a suboptimal solution by applying Taylor's first-order approximation. Finally, we discuss the condition under which the obtained solution is optimal. It provides a reference for the parameter selection in practical.

A. Problem Transformation

In this subsection, we will transform the proposed problem for analyzing more intuitively.

Firstly, we consider the constraints of effectiveness. The intervals that x should satisfy are shown visually in Fig. 2. It is obvious that $R_1(x)$ is monotonically decreasing because a larger x means less power to be allocated to U_1. On the other hand, $R_2(x)$ is monotonically increasing. In the extreme
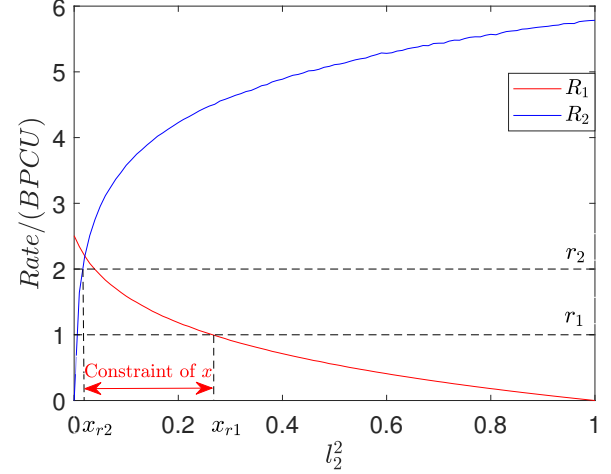
(a) Rates
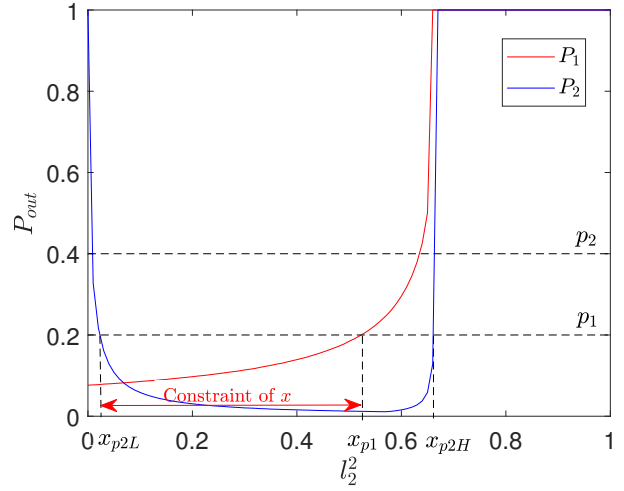
(b) P_{out}

Fig. 2. Rates and outage probabilities vs l_2^2 with the constraints.

case where all power is allocated to one user (i.e., $x = 0$ or $x = 1$), the rates can be calculated as follows:

$$R_1(0) = \frac{N}{2}\left(\log(1 + \frac{1}{C_1}) + J(\frac{C_1}{C_1 + 1}) - J(1)\right),$$
$$R_2(1) = \frac{N}{2}\left(J(1 + \frac{1}{C_1}) - J(1)\right), R_1(1) = R_2(0) = 0. \tag{40}$$

Then the constraints $R_1 \geq r_1$, $R_2 \geq r_2$ can be calculated as follows:

$$x_{r2} \leq x \leq x_{r1}, \tag{41}$$

where

$$x_{r1} = \begin{cases} R_1^{-1}(r_1), & r_1 < R_1(0) \\ 0, & r_1 \geq R_1(0) \end{cases}. \tag{42}$$

$$x_{r2} = \begin{cases} R_2^{-1}(r_2), & r_2 < R_2(1) \\ 0, & r_2 \geq R_2(1) \end{cases}, \tag{43}$$

$R_i^{-1}(r)$ is the inverse function of $R_i(x)$. The value of $R_i^{-1}(r_i)$ can be obtained by bisection search.

Then we consider the constraints of reliability. For brevity, $P_{out,1}, P_{out,2}$ will be denoted by P_1, P_2 below. Since $G(\omega)$ is a monotonically increasing function, we can know from (31) and (33) that $P_1(x)$ is monotonically non-decreasing. When $x = 0$, $P_1(x)$ reaches a minimum as

$$P_1(0) = G(\frac{C_1 T_1 1}{1 - C_1 T_1}). \tag{44}$$

The piecewise function $P_2(x)$ is monotonically non-increasing before C_T, and then non-decreasing in the condition of $C_2 \geq \frac{1}{T_1+T_2+T_1T_2}$. In this case, the minimum of $P_2(x)$ is

$$P_2(C_T) = 1 - G(\frac{C_T - C_2 T_2}{C_2 T_2}). \tag{45}$$

Otherwise, when $C_2 < \frac{1}{T_1+T_2+T_1T_2}$, $P_2(x)$ is a constant function as $P_2(x) = 1$. To combine these two cases, we set

$$P_2(C_T)' = \begin{cases} 1 - G(\frac{C_T - C_2 T_2}{C_2 T_2}), C_2 \geq \frac{1}{T_1 + T_2 + T_1 T_2} \\ 1, C_2 < \frac{1}{T_1 + T_2 + T_1 T_2} \end{cases}. \tag{46}$$

Then the constraints $P_1 \leq p_1$, $P_2 \leq p_2$ can be calculated as follows:

$$x_{p2L} \leq x \leq \min\{x_{p1}, x_{p2H}\}, \tag{47}$$

where

$$x_{p1} = \begin{cases} \dfrac{1 - C_1 T_1(1 + (G^{-1}(p_1))^{-1})}{T_1 + 1}, p_1 > P_1(0) \\ 0, p_1 \leq P_1(0) \end{cases}. \tag{48}$$

$$x_{p2L} = \begin{cases} C_2 T_2 G^{-1}(1 - p_2) + 1, p_2 > C_T \\ 1, p_2 \leq P_2(C_T)' \end{cases}, \tag{49}$$

$$x_{p2H} = \begin{cases} \dfrac{1 - C_2 T_1(1 + G^{-1}(1 - p_2))}{T_1 + 1}, p_2 > C_T \\ 0, p_2 \leq P_2(C_T)' \end{cases}. \tag{50}$$

$G^{-1}(p)$ is the inverse function of $G(\omega)$. The value of $G^{-1}(p_i)$ can be also obtained by bisection search.

After removing the independent terms of l_2 from $-R_1 - R_2$, P1 can be equated to the following problem:

$$\text{P}_2 : \min_x f(x) \tag{51}$$
$$\text{s.t. } x_L \leq x \leq x_H,$$

where

$$f(x) = \log(C_1 + x) + J(\frac{C_1}{C_1 + x}) - J(1 + \frac{x}{C_2}), \tag{52}$$

$$x_L = \max\{x_{r2}, x_{p2L}\}, x_H = \min\{x_{r1}, x_{p1}, x_{p2H}\}. \tag{53}$$

B. The Suboptimal Algorithm

In this subsection, we offer a suboptimal algorithm for the proposed problem. We propose an optimal algorithm and a suboptimal algorithm for two different cases, respectively. At last, we unify them into a suboptimal algorithm.

1) The optimal solution when the optimality condition holds: To find the extremum of the objective function to solve the proposed problem, we analyze the monotonicity of $f(x)$. It can be proved that $f(x)$ is monotonically decreasing when a certain condition holds, which is shown as the following theorem:

Theorem 6. $f(x)$ *is monotonically decreasing when*

$$\frac{C_1}{C_2} > \frac{1}{2} \left(\frac{d}{dx} J(1 + \frac{1}{C_2}) \right)^{-1}. \tag{54}$$

Proof. See Appendix H. ∎

According to the above analysis, when $\frac{C_1}{C_2} > \frac{1}{2} \left(\frac{d}{dx} J(1 + \frac{1}{C_2}) \right)^{-1}$, the optimal solution $x^* = x_H$. However, when the condition doesn't hold, we need to solve it by using another method.

2) The suboptimal solution when the optimality condition does not hold: When $\frac{C_1}{C_2} < \frac{1}{2} \left(\frac{d}{dx} J(1 + \frac{1}{C_2}) \right)^{-1}$, the function $f(x)$ is non-convex, which is difficult to solve. Thus, we apply the first-order Taylor expansion to approximate it in order to get a suboptimal solution x^*. The first-order Taylor expansion of $f(x)$ is expressed as follows:

$$\begin{aligned} f(x) &\approx f(0) + f'(x)x \\ &= \log C_1 + (\frac{1}{C_1} - \frac{1}{C_1}\frac{d}{dx}J(1) - \frac{1}{C_2}\frac{d}{dx}J(1))x. \end{aligned} \tag{55}$$

Then it can be shown that when $\frac{C_1}{C_2} > \left(\frac{d}{dx} J(1) \right)^{-1} - 1$, $f'(x)$ is monotonically decreasing, i.e, $x^* = x_H$. Otherwise, $f_1'(x)$ is monotonically increasing, and $x^* = x_L$.

After determining the optimal solution, we can calculate x_L and x_H by applying the bisection search. According to the above analysis, we design a suboptimal power allocation algorithm as IV-B2.

Algorithm 1 Suboptimal Power Allocation Algorithm

Input: $C_1, C_2, r_1, r_2, p_1, p_2, M, N$
Output: l_2^{2*}, when l_2^{2*} does not exist, output $l_2^{2*} = -1$.
1: Obtain $R_1^{-1}(r_1)$, $R_2^{-1}(r_2)$, $G^{-1}(p_1)$, $G^{-1(1-p_2)}$ by using bisection search, respectively.
2: Obtain $x_{r1}, x_{r2}, x_{p1}, x_{p2L}, x_{p2H}$ from (42), (43), (48), (49), (50), respectively.
3: $x_L = \max\{x_{r2}, x_{p2L}\}, x_H = \min\{x_{r1}, x_{p1}, x_{p2H}\}$
4: **if** $x_L \geq x_H$ **then**
5:      $l_2^{2*} = -1$
6: **else**
7:      **if** $\frac{C_1}{C_2} > \max\{(\frac{1}{2}\frac{d}{dx}J(1 + \frac{1}{C_2}))^{-1}, \left(\frac{d}{dx}J(1)\right)^{-1} - 1\}$ **then**
8:          $l_2^{2*} = x_H$
9:      **else**
10:          $l_2^{2*} = x_L$
11: **return** l_2^{2*}

Then we can analyze the complexity of the algorithm. Since all operations of the algorithm except the dichotomy are single operations, only the complexity of the dichotomy need to be considered. The precision requirement of l_2^{2*} is assumed to

TABLE II
PARAMETERS OF THE CHANNEL OF SIMULATION.

N_0	d_0	d_1	d_2	τ
-50dBm	1000m	1000m	800m	2

be ϵ, then the complexity of the dichotomy can be known as $O(\log \frac{2}{\epsilon})$. The complexity of the algorithm is $4O(\log \frac{2}{\epsilon})$.

In this subsection, we present a suboptimal power allocation algorithm. However, when condition (54) holds, the algorithm offers the optimal solution, which is what we expect. We are interested in the possibility that this condition holds to judge the practicability of the algorithm. We will discuss this in the next subsection.

C. Discussions of the optimality

In this subsection, we will analyze the condition term (54).

Since (54) is not direct-viewing, i.e., it doesn't give us any clear condition for optimality, we need to deal with $J(x)$ and get an estimated expression. From the definition of $J(x)$, the right side of the inequality can be transformed as follows:

$$\frac{d}{dx}J(1 + \frac{P_0}{d_2^\tau N_0}) = \int_0^{+\infty} \frac{1}{\omega + 1 + \frac{P_0}{d_2^\tau N_0}} g(\omega) d\omega. \tag{56}$$

In practice, $\frac{P_0}{N_0} >> d_2^\tau$. Then the approximation of (56) can be expressed as follows:

$$\frac{d}{dx}J(1 + \frac{P_0}{d_2^\tau N_0}) \approx \int_0^{+\infty} \frac{d_2^\tau N_0}{P_0} g(\omega) d\omega \tag{57}$$
$$= C_2.$$

Then inequality (54) can be transformed as follows:

$$C_1 > \frac{1}{2}. \tag{58}$$

By substituting (16) into C_1, (58) can be rewrited as follows:

$$\begin{cases} P_0 \in \mathbb{R}^+, \ P_R > 2MN d_1^\tau N_0 \\ P_0 < 2\dfrac{d_0^\tau N_0(NP_R + d_1^\tau N_0)}{P_R - 2MN d_1^\tau N_0}, \text{otherwise} \end{cases}. \tag{59}$$

(59) can be used to select an appropriate transmitting power to get optimal results. We will discuss this further in the next section.

V. SIMULATION

In this section, simulation results are presented to intuitively verify the proposed analytical results. The system parameters of the channels are chosen as Tab. II. All the numerical results are obtained from 10^6 times of simulation experiments with Matlab.

Fig. 3 presents the average rates of the users $(R_1 + R_2)/2$ achieved by GSVD-NOMA, the MIMO-NOMA schemes in [5], and the traditional OMA scheme, respectively. The transmission powers are chosen as $P_0 = P_R = P$, and the power allocation coefficient is set as $l_2^2 = 0.13$. The unit of the data rate here is 'bit per channel use' (BPCU). It can be observed from the figure that the GSVD-NOMA scheme has higher data rates. Besides, as the transmission power increases, the gaps of the rates of GSVD-NOMA and the other schemes also
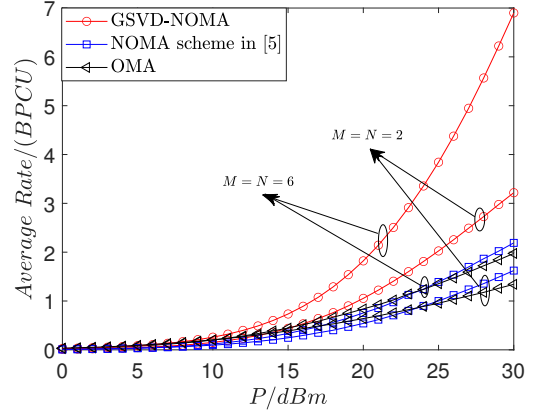

Fig. 3. The average rates achieved by the GSVD-NOMA, the MIMO-NOMA schemes in [5], and the OMA scheme, respectively.
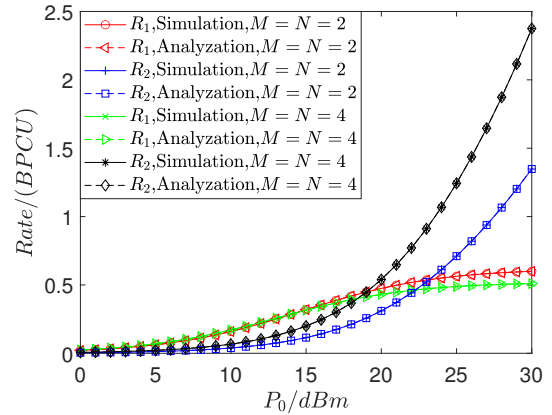

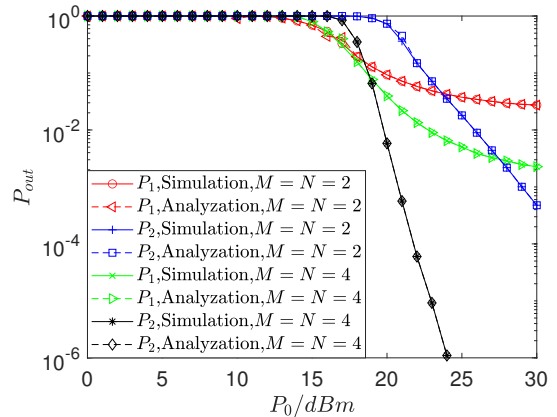Fig. 4. Analytical and simulation results of rates vs P_0 at different M, N.

Fig. 5. Analytical and simulation results of outage probabilities vs P_0 at different M, N.
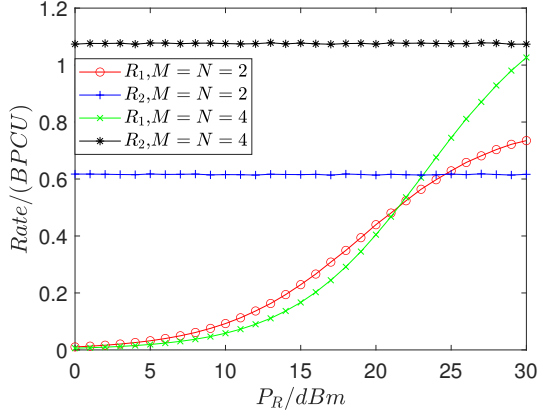
Fig. 6. Analytical and simulation results of rates vs P_R at different M, N.
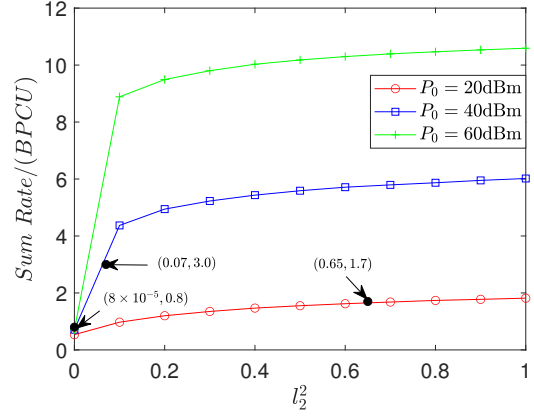

Fig. 8. Sum rates vs l_2^2 with different P_0.
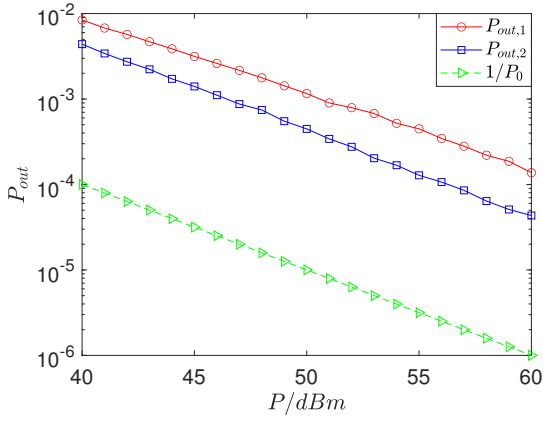

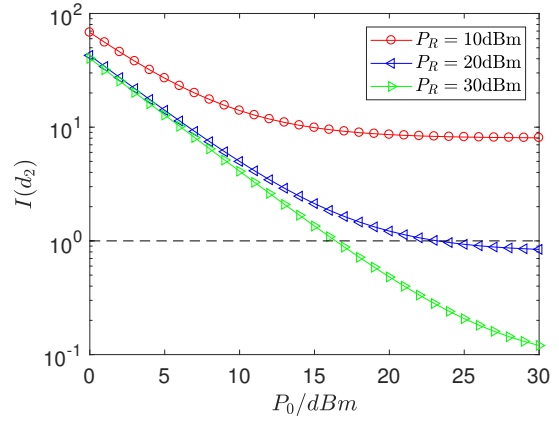Fig. 7. Outage probabilities at a high SNR condition.

Fig. 9. $I(d_2)$ vs P_0 with different P_R.

increase, demonstrating the great advantage of GSVD at high SNR.

Fig. 4 and 5 present the simulation and analytical average rates and outage probabilities of two users with 2×2 and 4×4 antennas, respectively. The transmission powers are chosen as $P_0 = P$ and $P_R = 20$ dBm is a constant. The target SINRs are set as $T_1 = T_2 = 1$. The results verify the accuracy of Theorem 3 and 4, respectively. It can also be observed that a larger number of antennas leads to higher average rates and lower outage probabilities, which are confirmed by the simulation figure. In practice, we can improve communication efficiency by increasing the number of antennas. Besides, the effect of P_0 on U_1 is far less than that of U_2. It is because the performance of U_1 is limited by the relay transmission power P_R. To study the effect of relay transmission power P_R, Fig. 6, the diagram of rates vs P_R at different M, N, is presented. The transmission power in BS is set as $P_0 = 20$dBm. It can be seen from the figure that P_R has no effect on U_2. On the other hand, P_R is decisive to the performance of U_1, which matches the actual circumstances.

As for asymptotic results from Theorem 5, Fig. 7 presents the simulation results of the outage probabilities at a high SNR condition. The antennas are chosen as 2×2. For the analysis of decay rate, the reference curve of $\frac{1}{P}$ is also presented in

the figure. As can be seen from the figure, the curves of both P_1 and P_2 are approximately parallel to the curve of $\frac{1}{P}$, i.e., P_{out_1}, $P_{out_2} \propto \frac{1}{P}$. These results are consistent with (90) and verify the asymptotic results of P_{out}.

Fig. 8 shows the sum rates vs l_2^2 with different p_0. It can be seen from the figure that the sum rate increases monotonically. According to Algorithm 1, we can get the optimal solution of l_2^{2*} as $l_2^{2*} = x_L$, respectively. We choose the required minimal rates and maximal outage probabilities as $r_1 = 0.2$, $r_2 = 1.5$, $p_1 = p_2 = 0.5$. Then we obtain these results by using bisection search and present them as points in the figure.

To verify the discussions of optimality of Algorithm 1 from Subsection IV-C, Fig. 9 is presented and shows the graph of the function

$$I(d_2) = \frac{C_1}{C_2} \Big/ \frac{1}{2} \left(\frac{d}{dx} J(1 + \frac{1}{C_2}) \right)^{-1} \tag{60}$$

vs P_0 with different P_R. To verify the results, we can obtain the range of P_0 by solving (59) directly: when $P_R = 10$dBm, $P_0 \in \mathbb{R}^+$; when $P_R = 20$dBm, $P_0 < 23$dBm; when $P_R = 30$dBm, $P_0 < 16.4$dBm. It can be seen from the figure that the threshold d_2 of $I(d_2) > 1$ is approximately equal to these three theoretical values. This demonstrates the accuracy of our analysis results about optimality.

VI. Conclusion

In this paper, an AF relay-assisted MIMO-NOMA transmission scenario with two IoT users was considered. The expressions of the marginal PDF the GSVs of two channel matrices were calculated and applied to the performance analysis. Specifically, the expressions of average rates, outage probabilities, and the asymptotic results of outage probabilities at high SNR were calculated, respectively. A suboptimal Algorithm was also proposed to maximize the sum rate within the constraints of communication quality requirements. The optimality conditions of the proposed algorithm are also obtained. Simulation results showed the superiority of the scheme and verified the conclusions above.

APPENDIX A
PROOF OF THEOREM 1

To facilitate the proof, first define the following matrix:

$$\mathbf{L} = (\mathbf{H}_1\mathbf{H}_0)^H (\mathbf{H}_1\mathbf{H}_0)(\mathbf{H}_2^H\mathbf{H}_2)^{-1}. \tag{61}$$

From (6), it can be inferred that

$$\begin{aligned}
\mathbf{L} &= \mathbf{V}^H \mathbf{\Sigma}_1^H \mathbf{\Sigma}_1 \mathbf{\Sigma}_2^{-1} \mathbf{\Sigma}_2^{-H} \mathbf{V}^{-H} \\
&= \mathbf{V}^H diag\{\omega_1, \omega_2, ..., \omega_N\} \mathbf{V}^{-H}.
\end{aligned} \tag{62}$$

(62) is written in terms of eigenvalue decomposition. It can be shown that the joint PDF of $\omega_1, \omega_2, ..., \omega_N$ equals the joint PDF of eigenvalues of $\mathbf{L}$. Because the matrix multiplication exchange order does not change the non-zero eigenvalues, the eigenvalues of $\mathbf{L}$ are equal to the eigenvalues of

$$\begin{aligned}
\mathbf{L}' &= (\mathbf{H}_2^\dagger)^H (\mathbf{H}_1\mathbf{H}_0)^H (\mathbf{H}_1\mathbf{H}_0)\mathbf{H}_2^\dagger \\
&= ((\mathbf{H}_1\mathbf{H}_0)\mathbf{H}_2^\dagger)^H ((\mathbf{H}_1\mathbf{H}_0)\mathbf{H}_2^\dagger).
\end{aligned} \tag{63}$$

From the [34], a Lemma can be known as follow:

Lemma 1. *Define a matrix*

$$\mathbf{X} = \mathbf{G}_r\mathbf{G}_{r-1}...\mathbf{G}_1(\hat{\mathbf{G}}_s\hat{\mathbf{G}}_{s-1}..\hat{\mathbf{G}}_1)^{-1}, \tag{64}$$

where $\mathbf{G}_k \in \mathbb{C}^{n_k \times n_{k-1}}$ and $\hat{\mathbf{G}}_k \in \mathbb{C}^{\hat{n}_k \times \hat{n}_{k-1}}$ are Gaussian random matrices with zero means and unit variances. $n_0 = \hat{n}_0 = \hat{n}_s = N$, $n_k = N + v_k$, $\hat{n}_k = N + \hat{v}_k$. Then the joint PDF of the non-zero eigenvalues of $\mathbf{XX}^H$ can be obtained as follows:

$$f(\omega_1, \omega_2, ..., \omega_N) = \frac{1}{V} \prod_{1 \leq m < n \leq N} (\omega_n - \omega_m) \det(\{G_{m,n,v,\hat{v}}\}). \tag{65}$$

$G_{m,n,v,\hat{v}}$ *is defined as follows:*

$$G_{m,n} = G_{s,r}^{r,s} \left(\begin{array}{c} \hat{v}_1', \hat{v}_2', ..., -\hat{v}_s' \\ v_1, v_2, ..., v_r \end{array} \middle| \omega_n \right), \tag{66}$$

where $\hat{v}_1' = -(\hat{v}_1 + m - 1 + N)$, $\hat{v}_t' = -(\hat{v}_t + N)$, $t = 2, 3, ..., s$.

Then the joint PDF of the non-zero eigenvalues of $\mathbf{L}'$ can be straightforwardly obtained via Lemma 1, and further obtain the results of the theorem.

APPENDIX B
PROOF OF THEOREM 2

$\prod_{1 \leq m < n \leq N} (\omega_n - \omega_m)$ can be rewritten as a Vandermonde determinant [35] as follows:

$$\begin{aligned}
\prod_{1 \leq m < n \leq N} (\omega_n - \omega_m) &= \begin{bmatrix} 1 & \omega_1 & \cdots & \omega_1^{N-1} \\ 1 & \omega_2 & \cdots & \omega_2^{N-1} \\ \vdots & \vdots & \ddots & \vdots \\ 1 & \omega_N & \cdots & \omega_N^{N-1} \end{bmatrix} \\
&= \sum_{\xi_1 \in S_N} sign(\xi_1) \prod_{o=1}^N \omega_o^{\xi_1(o)-1}
\end{aligned} \tag{67}$$

Then by expanding (67) and the determinant $\det(\{G_{m,n}\}) = \sum_{\xi_2 \in S_N} sign(\xi_2) \prod_{o=1}^N G_{\xi_2(o),o}$, (1) can be expressed as follows:

$$\begin{aligned}
f(\omega_1, \omega_2, ..., \omega_N) = &\sum_{\xi_1, \xi_2 \in S_N} sign(\xi_1)sign(\xi_2) \\
&\times \prod_{o=1}^N \omega_o^{N-\xi_1(o)} G_{\xi_2(o),o}.
\end{aligned} \tag{68}$$

The expression for marginal PDF is obtained by integrating (68) as follows:

$$\begin{aligned}
f(\omega_N) = &\sum_{\xi_1, \xi_2 \in S_N} sign(\xi_1)sign(\xi_2) \\
&\times \prod_{o=1}^{N-1} \int_0^{+\infty} \omega_o^{\xi_1(o)-1} G_{\xi_2(o),o} d\omega_o \omega_N^{\xi_1(N)-1} G_{\xi_2(N),N}.
\end{aligned} \tag{69}$$

From [36], $\int_0^{+\infty} \omega_o^{\xi_1(o)-1} G_{\xi_2(o),o} d\omega_o$ can be simplified as follows:

$$\begin{aligned}
&\int_0^{+\infty} \omega_o^{N-\xi_1(o)} G_{\xi_2(o),o} d\omega_o \\
&= \Gamma(\xi_1(o))\Gamma(M - N + \xi_1(o) + \xi_2(o) - 1)\Gamma(N - \xi_1(o) + 1).
\end{aligned} \tag{70}$$

Then we can get the result of the theorem.

APPENDIX C
PROOF OF THEOREM 1

When $M = N = 1$, (20) can be rewritten as follows:

$$\begin{aligned}
g(\omega) &= G_{1,2}^{2,1} \left(\begin{array}{c} -1 \\ 0, 0 \end{array} \middle| \omega \right) \\
&= \frac{1}{2\pi j} \int_L \Gamma(-u)^2 \Gamma(u+2) \omega_n^u du.
\end{aligned} \tag{71}$$

Since all poles of $\Gamma(-u)^2$ are to the right of the vertical axis in the complex plane, and all poles of $\Gamma(u+2)$ are to the left of the vertical axis in the complex plane. By the definition of the Meijer G-function, we can choose the integral path L as $L = [-j\infty, +j\infty]$. Then from [35], $G_{m,n}$ can be calculated as follows:

$$\begin{aligned}
g(\omega) &= \frac{1}{2\pi j} \int_{-j\infty}^{+j\infty} \Gamma(-u)^2 \Gamma(u+2) \omega_n^u du \\
&= U(2, 1, \omega_n).
\end{aligned} \tag{72}$$

Then the proof is completed.

APPENDIX D
PROOF OF THEOREM 1

The results of definite integrals used in this proof are all referenced from [35].

Since the modular square of a Gaussian random variable is subject to the exponential distribution, we can rewrite (23) as follows:

$$g(\omega_0) = \frac{x_0 x_1}{x_2}, \tag{73}$$

where x_i, $i = 0, 1, 2$ is the exponential random variable with the unit rate parameter. Then by using the result of the product distribution, the PDF of $z = x_1 x_2$ can be expressed as follows:

$$f(z) = \int_0^{+\infty} e^{-x} e^{-\frac{z}{x}} \frac{1}{x} dx \tag{74}$$
$$= 2 K_0(2\sqrt{z}),$$

where $K_0(x)$ is the modified Bessel function of the second kind [37]. Then we apply the result of ratio distribution to $\omega_0 = \frac{z}{x_2}$ as follows:

$$f(\omega_0) = 2 \int_0^{+\infty} x e^{-x} K_0(2\sqrt{x\omega_0}) dx \tag{75}$$
$$= \omega_0^{-\frac{1}{2}} e^{\frac{1}{2}\omega_0} W_{-\frac{3}{2},0}(\omega_0),$$

where $W_{-\frac{3}{2},0}(x)$ is the Whittaker function [38]. Then by expanding the Whittaker function into a definite integral, $f(\omega_0)$ can be rewritten as follows:

$$f(\omega_0) = \omega_0^{-\frac{1}{2}} e^{\frac{1}{2}\omega_0} \omega_0^{\frac{1}{2}} e^{-\frac{1}{2}\omega_0} \int_0^{+\infty} e^{-\omega_0 t} \frac{t}{(1+t)^2} dt$$
$$= \int_0^{+\infty} e^{-\omega_0 t} \frac{t}{(1+t)^2} dt \tag{76}$$
$$= U(2, 1, \omega_0).$$

The corollary is proved completely.

APPENDIX E
PROOF OF THEOREM 3

First, we define $J(x)$ as follows:

$$J(x) = \int_0^{+\infty} \log(\omega + x) g(\omega) d\omega. \tag{77}$$

$\log(\omega + x)$ can be expressed by Meijer-G function as follows:

$$\log(\omega + x) = \log x + \log(1 + \frac{\omega}{x})$$
$$= \log x + G_{2,2}^{1,2}\left(\begin{matrix} 1,1 \\ 1,0 \end{matrix} \middle| \frac{\omega}{x}\right). \tag{78}$$

Then $J(x)$ can be calculated as follows:

$$J(x) = \log x \int_0^{+\infty} g(\omega) d\omega + \int_0^{+\infty} G_{2,2}^{1,2}\left(\begin{matrix} 1,1 \\ 1,0 \end{matrix} \middle| \frac{\omega}{x}\right) g(\omega) d\omega$$
$$= \log x$$
$$+ \sum_{\xi_1,\xi_2 \in S_N} sign(\xi_1) sign(\xi_2) \prod_{o=1}^{N-1} W_o \int_0^{+\infty} G_{2,2}^{1,2}\left(\begin{matrix} 1,1 \\ 1,0 \end{matrix} \middle| \frac{\omega}{x}\right)$$
$$\times G_{1,2}^{2,1}\left(\begin{matrix} \xi_1(N) - N - 1 \\ M - N + \xi_1(N) + \xi_2(N) - 2, \xi_1(N) - 1 \end{matrix} \middle| \omega\right) d\omega. \tag{79}$$

From [35], the definite integral of the product of two Meijer-G functions over the positive axis transforms a Meijer-G function. Then $J(x)$ can be simplified as follows:

$$J(x) = \log x + \sum_{\xi_1,\xi_2 \in S_N} sign(\xi_1) sign(\xi_2) \prod_{o=1}^{N-1} W_o x G_{3,4}^{4,2}$$
$$\left(\begin{matrix} -1, \xi_1(N) - N - 1, 0 \\ -1, -1, M - N + \xi_1(N) + \xi_2(N) - 2, \xi_1(N) - 1 \end{matrix} \middle| x\right)$$
$$= \log x + \sum_{\xi_1,\xi_2 \in S_N} sign(\xi_1) sign(\xi_2) \prod_{o=1}^{N-1} W_o G_{3,4}^{4,2}$$
$$\left(\begin{matrix} 0, \xi_1(N) - N, 1 \\ 0, 0, M - N + \xi_1(N) + \xi_2(N) - 1, \xi_1(N) \end{matrix} \middle| x\right). \tag{80}$$

Then by substituting $J(x)$ into (25) and (26), R_1 and R_2 can be calculated as the expressions shown in the theorem.

Therefore, the proof for the theorem is complete.

APPENDIX F
PROOF OF THEOREM 4

Directly from the definitions, $P_{out,1}$ can be calculated as follows:

$$P_{out,1} = 1 - \Pr\{\frac{l_1^2 \omega_q}{(l_2^2 + C_1)\omega_q + C_1} > T_1\}$$
$$= 1 - \Pr\{((T_1 + 1)l_1^2 - T_1(C_1 + 1))\omega > C_1 T_1\}. \tag{81}$$

When $(T_1+1)l_1^2 - T_1(C_1+1) \le 0$, i.e., $l_2^2 \ge C_{H,1}$, $P_{out,1} = 1$. Otherwise,

$$P_{out,1} = 1 - \int_{D_1}^{+\infty} g(\omega) d\omega = G(D_1). \tag{82}$$

Similarly, $P_{out,2}$ can be calculated as follows:

$$P_{out,2} = 1 - \Pr\{\frac{l_1^2}{C_2\omega_q + C_2 + l_2^2} > T_1, \frac{l_2^2}{C_2\omega_q + C_2} > T_2\}$$
$$= 1 - \Pr\{\omega < \frac{(T_1 + 1)l_1^2 - T_1(C_2 + 1)}{C_2 T_1}, \omega < \frac{l_2^2 - C_2 T_2}{C_2 T_2}\}$$
$$= 1 - \Pr\{\omega < D_2^{-1}, \omega < E\}. \tag{83}$$

When $(T_1 + 1)l_1^2 - T_1(C_2 + 1) \le 0$ or $l_2^2 - C_2 T_2 < 0$, i.e., $l_2^2 \ge C_{H,2}$ or $l_2^2 \le C_2 T_2$, $P_{out,2} = 1$. Otherwise,

$$P_{out,2} = 1 - \int_0^{\min\{D_L^{-1}, E\}} g(\omega) d\omega$$
$$= \begin{cases} 1 - G(E), C_2 T_2 \le l_2^2 \le C_T \\ 1 - G(D_2^{-1}), C_T \le l_2^2 \le C_{H,2} \end{cases}. \tag{84}$$

Then we need to compare C_T with $C_2 T_2$ and $C_{H,2}$.

- When $C_2 < \frac{1}{T_1+T_2+T_1 T_2}$, we have the following equivalence relation:

$$C_2 < \frac{1}{T_1 + T_2 + T_1 T_2} \Leftrightarrow C_{H,2} > C_2 T_2$$
$$\Leftrightarrow C_T > C_2 T_2 \Leftrightarrow C_T < C_{H,2}. \tag{85}$$

Therefore, $P_{out,2}$ can be expressed as (33).
- When $C_2 \ge \frac{1}{T_1+T_2+T_1 T_2}$, $C_{H,2} \ge C_2 T_2$, $P_{out,2} = 1$.

As a result, the proof for the theorem is complete.

APPENDIX G
PROOF OF THEOREM 5

To obtain the asymptotic outage probabilities, we need to obtain the asymptotic characteristic of $G(\omega)$ of (35) first.

- When $\omega \to 0$, we can directly write the first order Taylor expansion of $G(\omega)$ at $\omega = 0$ as follows:

$$G(\omega) \approx G(0) + g(0)\omega = g(0)\omega. \tag{86}$$

- When $\omega \to +\infty$, it is difficult to get the asymptotic result of $G(\omega)$ directly. We will transform $G(\omega)$ to a definite integral of two Meijer-G functions' product. Specifically, $G(\omega)$ can be rewritten as follows:

$$
\begin{aligned}
G(\omega) &= \sum_{\xi_1,\xi_2 \in S_N} sign(\xi_1)sign(\xi_2) \prod_{o=1}^{N-1} W_o \\
&\times \int_0^{+\infty} G_{2,1}^{1,1}\left(\begin{matrix} M - N + \xi_1(N) + \xi_2(N) - 1, \xi_1(N) \\ -1 \end{matrix} \Big| t \right) \\
&\quad G_{1,1}^{1,1}\left(\begin{matrix} \xi_1(N) - N \\ 0 \end{matrix} \Big| \omega t \right) dt \\
&= \sum_{\xi_1,\xi_2 \in S_N} sign(\xi_1)sign(\xi_2) \prod_{o=1}^{N-1} W_o \\
&\times \int_0^{+\infty} G_{2,1}^{1,1}\left(\begin{matrix} M - N + \xi_1(N) + \xi_2(N) - 1, \xi_1(N) \\ -1 \end{matrix} \Big| t \right) \\
&\quad \Gamma(1 - \xi_1(N) + N)\frac{1}{(\omega t + 1)^{1 - \xi_1(N) + N}} dt.
\end{aligned} \tag{87}
$$

When $\omega \to +\infty$, $\omega t + 1 \to \omega t$, then $G(\omega)$ can be expressed as follows:

$$
\begin{aligned}
G(\omega) &= \sum_{\xi_1,\xi_2 \in S_N} sign(\xi_1)sign(\xi_2) \prod_{o=1}^{N-1} W_o \\
&\times K_{\xi_1,\xi_2} \frac{1}{\omega^{1 - \xi_1(N) + N}} \approx K\frac{1}{\omega}
\end{aligned} \tag{88}
$$

where K_{ξ_1,ξ_2}, K are coefficients independent of ω. Here we omit the higher order terms of $\frac{1}{\omega}$, because $(\frac{1}{\omega})^n << \frac{1}{\omega}$ when $n \geq 2$.

From (16) and (34), it can be shown that when $P_0 \to +\infty$, $D_1 \to \frac{1}{P_0}$, $D_2 \to P_0, E \to P_0$. Then by substituting these into the definitions of P_{out}, we have

$$P_{out,1} \to G(\frac{1}{P_0}), \; P_{out,2} \to G(P_0). \tag{89}$$

From (86) and (88), the asymptotic results of $P_{out,1}$ and $P_{out,2}$ can be obtained as follows:

$$P_{out,1} \to \frac{1}{P_0}, \; P_{out,2} \to \frac{1}{P_0}. \tag{90}$$

Then the proof of the theorem is complete.

APPENDIX H
PROOF OF THEOREM 6

Since

$$\frac{d^2 J(x)}{dx^2} = -\int_0^{+\infty} \frac{1}{(\omega + x)^2} g(\omega)d\omega < 0, \tag{91}$$

it is known that $\frac{d}{dx}J(x)$ is monotonically decreasing. Then it can be inferred that

$$\frac{d}{dx}J(1 + \frac{x}{C_2}) > \frac{d}{dx}J(1 + \frac{1}{C_2}). \tag{92}$$

Then we can know that

$$
\begin{aligned}
&\frac{df(x)}{dx} \\
&= \frac{1}{C_1 + x} - \frac{C_1}{(C_1 + x)^2}\frac{d}{dx}J(\frac{C_1}{C_1 + x}) - \frac{1}{C_2}\frac{d}{dx}J(1 + \frac{x}{C_2}) \\
&< \frac{1}{C_1 + x} - \frac{1}{C_2}\frac{d}{dx}J(1 + \frac{1}{C_2}) = \frac{f_0(x)}{(C_1 + x)^2 C_2},
\end{aligned} \tag{93}
$$

where $f_0(x)$ is an inverted-U quadratic function as follows:

$$
\begin{aligned}
f_0(x) &= -\frac{d}{dx}J(1 + \frac{1}{C_2})x^2 + (C_2 - 2C_1\frac{d}{dx}J(1 + \frac{1}{C_2}))x \\
&\quad - C_1^2\frac{d}{dx}J(1 + \frac{1}{C_2}).
\end{aligned} \tag{94}
$$

When $\frac{C_1}{C_2} > \frac{1}{2}\left(\frac{d}{dx}J(1 + \frac{1}{C_2}) \right)^{-1}$, the axis of symmetry

$$-\frac{C_2 - 2C_1\frac{d}{dx}J(1 + \frac{1}{C_2})}{2 \times -\frac{d}{dx}J(1 + \frac{1}{C_2})} < 0. \tag{95}$$

Since $f_0(0) < 0$, it can be inferred that $f_0(0)$ is negative on the positive axis. On the other hand, $f(x)$ is monotonically decreasing. Then the proof of the theorem is completed.

REFERENCES

[1] A. Kaye and D. George, "Transmission of multiplexed PAM signals over multiple channel and diversity systems," *IEEE Transactions on Communication Technology*, vol. 18, no. 5, pp. 520–526, 1970.

[2] Y. Huang, C. Zhang, J. Wang, Y. Jing, L. Yang, and X. You, "Signal processing for MIMO-NOMA: Present and future challenges," *IEEE Wireless Communications*, vol. 25, no. 2, pp. 32–38, 2018.

[3] B. M. Lee and H. Yang, "Massive MIMO with massive connectivity for industrial internet of things," *IEEE Transactions on Industrial Electronics*, vol. 67, no. 6, pp. 5187–5196, 2020.

[4] P. Liu and T. Jiang, "Channel estimation performance analysis of massive MIMO IoT systems with ricean fading," *IEEE Internet of Things Journal*, vol. 8, no. 7, pp. 6114–6126, 2021.

[5] Z. Ding, F. Adachi, and H. V. Poor, "The application of MIMO to non-orthogonal multiple access," *IEEE Transactions on Wireless Communications*, vol. 15, no. 1, pp. 537–552, 2016.

[6] Z. Ding, R. Schober, and H. V. Poor, "A general MIMO framework for NOMA downlink and uplink transmission based on signal alignment," *IEEE Transactions on Wireless Communications*, vol. 15, no. 6, pp. 4438–4454, 2016.

[7] Z. Chen, Z. Ding, X. Dai, and R. Zhang, "An optimization perspective of the superiority of NOMA compared to conventional OMA," *IEEE Transactions on Signal Processing*, vol. 65, no. 19, pp. 5191–5202, 2017.

[8] M. Zeng, A. Yadav, O. A. Dobre, G. I. Tsiropoulos, and H. V. Poor, "Capacity comparison between MIMO-NOMA and MIMO-OMA with multiple users in a cluster," *IEEE Journal on Selected Areas in Communications*, vol. 35, no. 10, pp. 2413–2424, 2017.

[9] U. Uyoata, J. Mwangama, and R. Adeogun, "Relaying in the internet of things (IoT): A survey," *IEEE Access*, vol. 9, pp. 132 675–132 704, 2021.

[10] D. Zhang, Y. Liu, Z. Ding, Z. Zhou, A. Nallanathan, and T. Sato, "Performance analysis of non-regenerative massive-MIMO-NOMA relay systems for 5G," *IEEE Transactions on Communications*, vol. 65, no. 11, pp. 4777–4790, 2017.

[11] M.-G. Bereeanu, C. Voicu, and S. Halunga, "AF relaying in a massive MU-MIMO OFDM system," in *2018 IEEE 24th International Symposium for Design and Technology in Electronic Packaging? (SIITME)*, 2018, pp. 226–229.

[12] X. Yue, Y. Liu, S. Kang, A. Nallanathan, and Z. Ding, "Exploiting full/half-duplex user relaying in NOMA systems," *IEEE Transactions on Communications*, vol. 66, no. 2, pp. 560–575, 2018.

[13] J. Laneman, D. Tse, and G. Wornell, "Cooperative diversity in wireless networks: Efficient protocols and outage behavior," *IEEE Transactions on Information Theory*, vol. 50, no. 12, pp. 3062–3080, 2004.

[14] B. Lee and C. Lee, "A joint precoding scheme for MIMO systems with distributed single antenna AF relays," in *2012 International Conference on ICT Convergence (ICTC)*, 2012, pp. 666–670.

[15] F. Heliot and R. Tafazolli, "Energy-efficient joint source and relay precoding design for cooperative MIMO-AF systems," in *2017 European Conference on Networks and Communications (EuCNC)*, 2017, pp. 1–6.

[16] J. L. Bing, L. Gopal, Y. Rong, C. W. R. Chiong, and Z. Zang, "Robust transceiver design for multi-hop AF MIMO relay multicasting from multiple sources," *IEEE Transactions on Vehicular Technology*, vol. 70, no. 2, pp. 1565–1576, 2021.

[17] M. Costa, "Writing on dirty paper (corresp.)," *IEEE transactions on information theory*, vol. 29, no. 3, pp. 439–441, 1983.

[18] H. Harashima and H. Miyakawa, "Matched-transmission technique for channels with intersymbol interference," *IEEE Transactions on Communications*, vol. 20, no. 4, pp. 774–780, 1972.

[19] A. Li and C. Masouros, "A two-stage vector perturbation scheme for adaptive modulation in downlink MU-MIMO," *IEEE Transactions on Vehicular Technology*, vol. 65, no. 9, pp. 7785–7791, 2016.

[20] C. Masouros, "Correlation rotation linear precoding for MIMO broadcast communications," *IEEE Transactions on Signal Processing*, vol. 59, no. 1, pp. 252–262, 2011.

[21] X. Zhang, Y. Qi, and M. Vaezi, "A rotation-based method for precoding in gaussian MIMOME channels," *IEEE Transactions on Communications*, vol. 69, no. 2, pp. 1189–1200, 2021.

[22] L. Gerdes, L. Weiland, and W. Utschick, "Optimal partial decode-and-forward rates for the gaussian MIMO relay channel using the GSVD," in *2014 IEEE 15th International Workshop on Signal Processing Advances in Wireless Communications (SPAWC)*, 2014, pp. 259–263.

[23] Z. Chen, Z. Ding, X. Dai, and R. Schober, "Asymptotic performance analysis of GSVD-NOMA systems with a large-scale antenna array," *IEEE Transactions on Wireless Communications*, vol. 18, no. 1, pp. 575–590, 2018.

[24] C. Rao, Z. Ding, and X. Dai, "The distribution characteristics of ordered GSVD singular values and its applications in MIMO-NOMA," *IEEE Communications Letters*, pp. 1–1, 2020.

[25] M. F. Hanif and Z. Ding, "Robust power allocation in MIMO-NOMA systems," *IEEE Wireless Communications Letters*, vol. 8, no. 6, pp. 1541–1545, 2019.

[26] C. Rao, Z. Ding, and X. Dai, "GSVD-based MIMO-NOMA security transmission," *IEEE Wireless Communications Letters*, vol. 10, no. 7, pp. 1484–1487, 2021.

[27] C. Rao, "Application of GSVD-based precoding in MIMO-NOMA relaying systems," *IET Communications*, vol. 14, pp. 3802–3812(10), December 2020.

[28] D. Tse and P. Viswanath, *Fundamentals of wireless communication*. Cambridge university press, 2005.

[29] A. M. Tulino, S. Verdú, and S. Verdu, *Random matrix theory and wireless communications*. Now Publishers Inc, 2004.

[30] C. F. Van Loan, "Generalizing the singular value decomposition," *SIAM Journal on numerical Analysis*, vol. 13, no. 1, pp. 76–83, 1976.

[31] R. Beals and J. Szmigielski, "Meijer G-functions: a gentle introduction," *Notices of the American Mathematical Society*, vol. 60, no. 7, pp. 866–873, 2013.

[32] F. Tricomi, "Sulle funzioni ipergeometriche confluenti," *Annali di Matematica Pura ed Applicata*, vol. 26, no. 1, pp. 141–175, 1947.

[33] 2001, October 29. [Online]. Available: http://functions.wolfram.com/07.34.21.0002.01

[34] P. J. Forrester, "Eigenvalue statistics for product complex wishart matrices," *Journal of Physics A*, vol. 47, no. 34, p. 345202, 2014.

[35] A. Jeffrey and D. Zwillinger, *Table of integrals, series, and products*. Elsevier, 2007.

[36] J. R. Ipsen, "Products of independent gaussian random matrices," *arXiv preprint arXiv:1510.06128*, 2015.

[37] M. Abramowitz and I. A. Stegun, *Handbook of mathematical functions with formulas, graphs, and mathematical tables*. US Government printing office, 1948, vol. 55.

[38] E. T. Whittaker, "An expression of certain known functions as generalized hypergeometric functions," *Bulletin of the American Mathematical Society*, vol. 10, no. 3, pp. 125–134, 1903.